Annals of Nuclear Energy 112 (2018) 411–417

Contents lists available at ScienceDirect

Annals of Nuclear Energy

journal homepage: www.elsevier.com/locate/anucene

Photon and neutron shielding features of quarry tuff

Hector Rene Vega-Carrillo [a,*], Karen Arlet Guzman-Garcia [b], Jose Antonio Rodriguez-Rodriguez [c,d], Cesar Antonio Juarez-Alvarado [d], Vishwanath P. Singh [e], Héctor Asael de León-Martinez [f]

[a] Universidad Autonoma de Zacatecas, Unidad Academica de Estudios Nucleares, Cipres 10, Fracc. La Peñuela, 98060 Zacatecas, Zac, Mexico
[b] Universidad Politecnica de Madrid, Departamento de Ingenieria Energetica, C. Jose Gutierrez Abascal 2, 28600 Madrid, Spain
[c] Universidad Autonoma de Zacatecas, Unidad Academica de Ingenieria, Av. Ramon Lopez Velarde s/n, 98068 Zacatecas, Zac, Mexico
[d] Universidad Autonoma de Nuevo Leon, Facultad de Ingenieria Civil, C. Pedro de Alba s/n, San Nicolas de los Garza, NL, Mexico
[e] Department of Physics, Karnatak University, Dharwad 580003, India
[f] Instituto Tecnológico de Aguascalientes, Av. Adolfo López Mateos 1801 Ote. Fracc. Bona Gens, 20155 Aguascalientes, Ags, Mexico

ARTICLE INFO

Article history:
Received 18 August 2017
Received in revised form 15 October 2017
Accepted 19 October 2017

Keywords:
Quarry tuff
Shielding
Photons
Neutrons
^{137}Cs
^{241}AmBe
MCNP5
XCOM

ABSTRACT

The shielding characteristics of quarry tuff (cantera) against photons and ^{241}AmBe neutrons, were determined. The effective atomic number of cantera, the Exposure and the Energy absorption buildup factors for photons in cantera were also calculated. The XCOM code was used to calculate the photon interaction coefficients. Also, Monte Carlo method was used to model a photon transmission experiment in cantera. Collided and uncollided photon fluence, Kerma in air, and Ambient dose equivalent were estimated. With the uncollided photon fluence the linear attenuation coefficients were determined and compared with those calculated with the XCOM code. The linear attenuation coefficient for 0.662 MeV photons was compared with the coefficient measured with a NaI(Tl)-based γ-ray spectrometer and a ^{137}Cs source. The Monte Carlo model was also used to estimate the neutron spectra of ^{241}AmBe neutrons in function of cantera thickness, the Effective and the Ambient dose equivalent for the collided and uncollided neutrons. Cantera has good shielding properties for low energy photons and poor shielding features against ^{241}AmBe neutrons.

1. Introduction

Nuclear radiation is widely used in several fields; its applications increase constantly because in the interaction with matter radiations produce a desired effect or useful and unique information. The common factors in these applications are the radiation source and the need to use radiation protection protocols where shielding is a compulsory item (Narici et al., 2017; Sayyed, 2016).

Among the applications of gamma radiations are to sterilize, food processing, medical diagnostics and therapy, elemental analysis, to evaluate the weld integrity in pipes or vessels working with high pressures, etc. Here, is important to avoid the radiation exposure using the adequate shielding (Kaur et al., 2016).

The prompt gamma neutron activation analysis (PGNAA) requires a neutron source and its shield, the sample to be analysed and a gamma-ray spectrometer. In this application neutrons produced by ^{252}Cf, ^{241}AmBe or 14 MeV neutron generator are used. In this application the shielding must deal with neutrons and gamma-rays. In the aim of maximize the neutron moderation and minimize the gamma-rays from the ^{252}Cf source, and those produced in the sample through (n, γ) reactions Hadad et al. (2016) designed the shielding using Monte Carlo methods.

Nuclear well logging tools are used in the oil logging industry to measure the porosity formation and the element concentration. In this application a neutron source is used requiring a compact shielding. A compact shielding tank, for a 0.67 TBq ^{241}AmBe source, was designed using Monte Carlo method. Anywhere outside the tank the total dose rate was less than 0.025 mSv/h (Zhang et al., 2017).

Efforts to determine the shielding features of different materials are constantly reported (El-Khayatt et al., 2014; El-Khayatt, 2017). The shielding characteristics of building materials (Singh et al., 2014; Mann et al., 2013), ores (Oto et al., 2015), glass (Kaewjang et al., 2014), plastics and polymers (Mann et al., 2015), and concrete with different aggregates (Waly and Bourham, 2015; Oto et al., 2016) have been carried out. In these works the shielding features were concerned about the effective atomic number, the effective electron density, the half value layer (HVL), the energy absorption and exposure buildup factors, the linear attenuation

* Corresponding author.
E-mail addresses: rvega@uaz.edu.mx (H.R. Vega-Carrillo), rrodrij@uaz.edu.mx (J.A. Rodriguez-Rodriguez), cesar.juarezal@uanl.edu.mx (C.A. Juarez-Alvarado).

https://doi.org/10.1016/j.anucene.2017.10.042
0306-4549/

coefficient (μ), and the mass attenuation coefficient (μ_m) for photons. The characterization has been carried out through measurements, calculations or combining both procedures. Singh et al., (2014) also include the shielding features against neutrons of building materials.

Concrete is a material widely used in the construction industry, also it is used as biological shielding because is effective to attenuate X-rays, γ-rays, and neutrons. Hormirad™ is a high-density concrete whose shielding features against ^{241}AmBe neutrons were studied through measurements and Monte Carlo calculations (Gallego et al., 2009). Neutron shielding features on NGS-concrete, polymer and standard cements mortars have been also reported (Piotrowski et al., 2015a, 2015b). Here, the half and the tenth-value layer were evaluated. Another features related with the shielding characteristics of materials are the Exposure Buildup Factor (EBF) and the Energy Absorption Buildup Factor (EABF). Wally et al. (2016) have studied the γ-ray shielding characteristics of different compositions of glasses having higher content of PbO and Bi_2O_3 which have better shielding properties in comparison to concrete. However, the EBF for these glasses is very large in comparison to concrete. Glasses made with higher concentration of silicon have EBF and EABF similar to the building factor than concrete (Mann, 2017). In the case of polymers and tissue substitute materials, the EBF and the EABF for low energy photons remain constant, whereas both building factors tend to increase with increasing penetration depths (Kurudirek and Ozdemir, 2011).

Soils and locally-abundant materials (dolomite, gypsum, igneous rock and lime stone), have been studied to be used as shielding. All samples have the same shielding effectiveness for 0.30–3.0 MeV photons, and it is related with the effective atomic number. Studied soils can be used for low-cost shielding as they are abundant (Mann et al., 2012).

Tuffs are volcanic rocks made of an ash matrix with grain sizes ranging from fine clay minerals up to silt-sized material. Quarry tuffs are mostly soft and porous rocks used as building stones and for artwork because can be easily cut and reworked. Volcanic tuff stones are in different colours, they are used as covering materials for insulating and ornamental purposes on the exterior and interior of buildings (López-Doncel et al., 2016; Wedekind et al., 2013; Degerlier, 2013; Turhan et al., 2015). In the construction industry the quarry tuff (hereinafter referred to as cantera) is used to coat the interior and exterior wall surfaces of buildings and houses avoiding the use of paint. Its use is part of the Mexico's stone heritage being present in pre-Hispanic, Colonial and modern architecture (Pérez et al., 2014). A radiometric analysis of this material from Turkey has been reported (Degerlier, 2013; Turhan et al., 2015), being in mostly of cases safe. In Mexico there are several cities where the cantera is widely used; however, its features to shield neutrons, X-or-γ photons are unknown, therefore in facilities with cantera hosting X-ray units or γ-ray sources cantera is not accounted for shielding design or evaluation.

The aim of this work was to determine the shielding characteristics of cantera. For 0.03, 0.07, 0.1, 0.3, 0.662, 1, 2, and 3 MeV mono-energetic photons, the linear attenuation coefficient (μ), and the mass attenuation coefficient (μ_m) were calculated using Monte Carlo methods and the XCOM code (Berger et al., 2015). The effective atomic number (Z_{eff}), the EBF, and the EABF were also calculated for various photon energies and depth penetrations. The relative transmission of Kerma in air, K_a, and the ambient dose equivalent, $H^*(10)$, was also determined. For 0.662 MeV photons, the calculated μ was compared with the μ measured with a NaI (Tl)-based γ-ray spectrometer and a ^{137}Cs source, using a narrow beam geometry. The neutron spectrum, the $H^*(10)$, and the effective dose for rotational geometry (E_{rot}) of ^{241}AmBe neutrons were also calculated.

Obtained information could be useful in the shielding evaluation in constructions using cantera as the main building material or as decorative complement in walls of facilities having X-ray equipment, γ-ray sources or ^{241}AmBe neutron sources.

2. Materials and methods

From the local market a large piece of cantera was purchased and it was cut in 10x10 cm pieces with different thickness, ranging from 1 up to 40 cm. Each piece was weighted to determine the density, being 1.8 ± 2% g cm^{-3}. Other pieces were selected to measure the chemical composition using Energy Dispersive X-ray Fluorescence technique with a spectrometer PANalytical, model Epsilon3-XL. Measurements were replicated five times using different pieces.

Cantera, is mainly composed by SiO_2, Al_2O_3, K_2O, Na_2O, Fe_2O_3, and CaO, being in agreement with the chemical composition reported by Celik and Ergul (2015). Due to the total alkali (Na_2O + K_2O) versus silica (SiO_2) composition, this quarry tuff is Rhyolite (Celik and Ergul, 2015; Le Bas et al., 1992).

2.1. Calculations

The elemental concentration, in weight fraction, of cantera was calculated being O (0.4604%), Si (0.2476%), Al (0.1022%), C (0.0651%), Fe (0.0509%), K (0.0459%), Na (0.0156%), Mg (0.0074%), and Ca (0.0049%). These data were used to calculate the shielding features against photons. Calculations were carried out with the XCOM and the MCNP5 (X-5 Monte Carlo Team, 2003) codes.

2.1.1. XCOM

With the XCOM code the partial mass interaction coefficients and the total mass attenuation coefficients, for 10^{-3}–10^{5} MeV photons, were calculated for cantera.

2.1.2. Effective atomic number

The effective atomic number ($\mathbf{Z_{eff}}$) of cantera, for 1.5E(-2) to 20 MeV photons, was calculated using Eq. (1).

$$Z_{eff} = \frac{\sum_i f_i A_i \mu_{mi}}{\sum_i f_i \frac{A_i}{Z_i} \mu_{mi}} \tag{1}$$

here, f_i is the atom fraction, Z_i is the atomic number, A_i is the atomic mass, and μ_{mi} is the total mass attenuation coefficient (μ/ρ) of the *i*th element in cantera.

2.1.3. Buildup factors

The Exposure and Energy absorption buildup factors, EBF and EABF respectively, for cantera were calculated for 0.015–15 MeV photons, and for penetration depths ranging from 0.015 to 40 mean free paths (mfp). Calculations were carried out using the Geometric-progression fitting parameters (G-P) for the elements in the cantera taken from the ANS (1991). Buildup factors for cantera were calculated using the five-parameter fitting formula for mixtures and compound reported by Harima et al. (1991) shown in Eqs. (2) and (3).

$$B(E,x) = \begin{cases} 1 + \frac{b-1}{K-1}(K^x - 1) & \text{for } K \neq 1 \\ 1 + (b-1)x & \text{for } K = 1 \end{cases} \tag{2}$$

$$K(E,x) = cx^a + d\frac{\tanh\left(\frac{x}{X_k} - 2\right) - \tanh(-2)}{1 - \tanh(-2)} \qquad \text{for } x \leq 40 \text{ mfp} \tag{3}$$

here, **E** is the photon energy, **x** is the penetration depth in mfp units, and **a**, **b**, **c**, **d** and $\mathbf{X_k}$ are the G-P fitting parameters. The value of

parameter **b** corresponds to that of the buildup factor at 1 mfp. The variation of the parameter **K** with the penetration depth ($\mathbf{K^x}$) represents the photon dose multiplication and the photon spectrum change.

2.1.4. Monte Carlo calculations

In the MCNP5 calculations a model of a transmission experiment was built. Here, a point-like and isotropic photon source was used where the source term was mono-energetic, with photons of 30, 70, 100, and 300 keV in order to cover the x-rays for diagnosis, and 0.662, 1, 2 and 3 MeV to include gamma-ray sources. A point-like detector was placed 42 cm from the source. Between the source and the detector, the cantera pieces where included. Calculations were carried out for 0, 0.5, 1, 2, . . ., 39, 40 cm-thick cantera pieces. The f5 tally was used to estimate the collided (total) and the uncollided photon fluence. The uncollided photon fluence and the cantera thickness were fitted to the exponential function in order to calculate the linear attenuation coefficients that were compared with the μ calculated with the XCOM code. In the MCNP5 calculations the Kerma in air, Ka, and the Ambient dose equivalent, H*(10) were also calculated using the ICRP 74 (1996) fluence-to-dose conversion coefficients. The amount of histories was 10^8 allowing to have uncertainties less than 5%.

The same model was used to calculate the shielding characteristics of cantera against ^{241}AmBe neutrons. Here, a point-like and isotropic source was modeled; the source term was taken from the compendium prepared by the IAEA (2001). The neutron spectra, the H*(10) and the E_{rot} were calculated in function of the cantera thickness.

2.2. Measurements

Using a 555 ± 5% MBq ^{137}Cs source in a lead shield (8 cm-diameter and 9 cm-length cylinder) with a 1 cm-diameter collimator, a transmission experiment was carried out using a narrow geometry array. The transmitted photon spectrum was measured with a 7.62 Ø × 7.62 cm NaI(Tl) detector. The detector was sited in a lead shield (16.5 cm-outer diameter and 2 cm thick) with a 3.5 cm-thick lead lid with 1 cm-diameter collimator. Both collimators were aligned being 42 cm apart. In the space in between cantera samples (10 x 10 cm with 1, 2, 3, 4, 5, 6, 7, 8, 9, 10 cm-thick), were allocated individually and combining different thickness.

The area under the 0.662 MeV photopeak was measured as the cantera pieces with different thickness were placed between the source and the detector. The live-time of measurements was set to get 1% uncertainty in the photopeak net area.

For each cantera thickness the net count rates under the 0.662 photopeak were corrected due to background. Corrected count rates were normalized to the count rate measured without cantera and adjusted to an exponential function using the weighted regression. Weights were the reciprocal of the sum of variances in the net count rates and the thickness of cantera (Vega-Carrillo, 1989).

3. Results

3.1. Calculations

3.1.1. XCOM

The partial mass interaction coefficients, for 10^{-3}–10^5 MeV photons, in cantera are shown in Fig. 1. These were calculated with the XCOM code.

Interaction coefficients include coherent and incoherent (Compton) scattering, photoelectric effect, as well as, nuclear and electron pair production. In cantera the photoelectric absorption

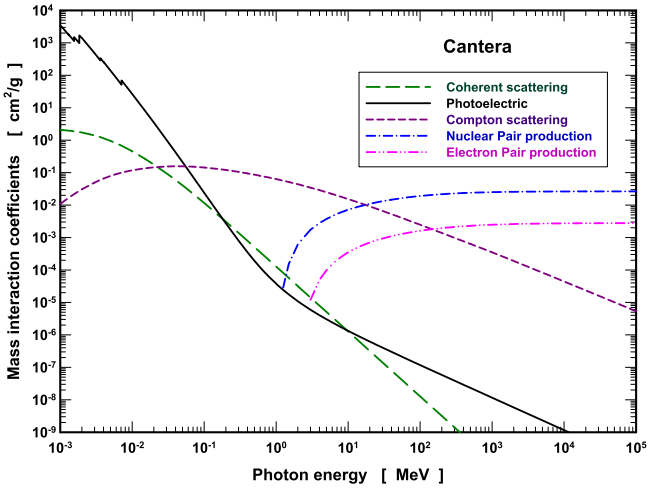

Fig. 1. Photon mass interaction coefficients in cantera.

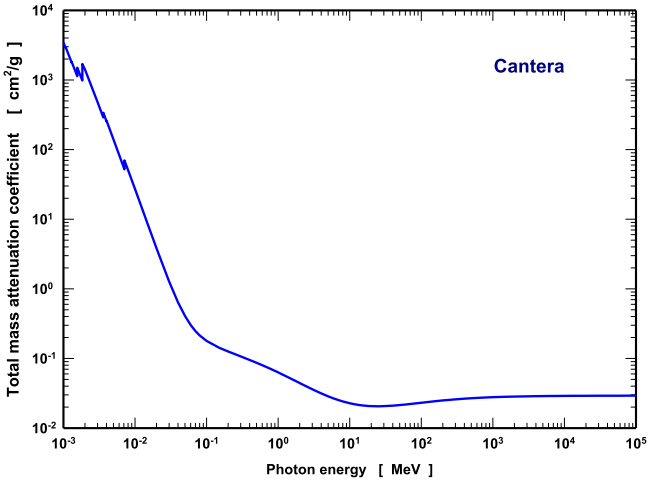

Fig. 2. Total mass attenuation coefficients of cantera.

is the main interaction mechanism for photons less than 60 keV, the best shielding performance is for low energy photons. For photons from 60 keV to approximately 20 MeV Compton scattering is the main interaction process with cantera where scattered photon, with lower energy, are produced.

The total mass attenuation coefficients are shown in Fig. 2.

In the low energy region there are 7 resonances due to K absorption edge in Na, Mg, Al, Si, K, Ca, and Fe. Using the mass attenuation coefficients and the density of cantera, the linear attenuation coefficients for 0.03, 0.07, 0.1, 0.3, 0.662, 1, 2 and 3 MeV photons were calculated.

3.1.2. Effective atomic number

The Z_{eff} of cantera, for 1.5E(-2) to 20 MeV photons is shown in Table 1. The Z_{eff} variation trend with the photon energy is alike to the Z_{eff} reported for concrete samples (Oto et al., 2016).

The largest values are for low-energy photons where the photoelectric absorption is the main interaction process. From 0.3 to 3 MeV the Z_{eff} values are reduced, this is the region where the Compton scattering is dominant. The lower Z_{eff} is noticed for 1 MeV photons. Above 4 MeV the Z_{eff} increases again being almost constant.

3.1.3. Buildup factors

The Exposure buildup factors for 1.5E(−2) to 15 MeV photons, and for 0.5–40 mfp penetration depths in cantera are shown in

Table 1
Effective atomic number of cantera.

Energy [MeV]	Z_{eff}
1.50E−02	15.623
2.00E−02	15.543
3.00E−02	14.858
4.00E−02	13.838
5.00E−02	12.852
6.00E−02	12.072
8.00E−02	11.101
1.00E−01	10.616
1.50E−01	10.167
2.00E−01	10.035
3.00E−01	9.955
4.00E−01	9.930
5.00E−01	9.920
6.00E−01	9.915
8.00E−01	9.909
1.00E+00	9.907
1.50E+00	9.908
2.00E+00	9.921
3.00E+00	9.964
4.00E+00	10.016
5.00E+00	10.070
6.00E+00	10.123
8.00E+00	10.224
1.00E+01	10.312
1.50E+01	10.482
2.00E+01	10.602

Fig. 3; meanwhile in Fig. 4 are shown the Energy absorption buildup factors. Both buildup factors have a Gaussian-like distribution skewed to photons with lower energy. The peaks tend to the right as the penetration depth is increased to the region where Compton scattering dominates producing photons that reach the detector.

3.1.4. Monte Carlo calculations

In Fig. 5 are shown the relative uncollided photon transmission, estimated with the MCNP5 code for monoenergetic photon sources in function of the mass thickness of cantera.

Data from Fig. 4 were fitted into exponential functions and the linear attenuation coefficients were calculated. In Table 2 are shown the μ values obtained with the XCOM and MCNP5 codes.

There is a good agreement between the μ calculated using both codes. The largest difference, noticed for 3 MeV photons, was 0.27% being statistically insignificant. Cantera HVL is 0.3, 1.6, 2.1, 3.6, 5.0, 6.1, 8.7, and 10.7 cm for 0.03, 0.07, 0.1, 0.3, 0.662, 1, 2, and 3 MeV photons respectively.

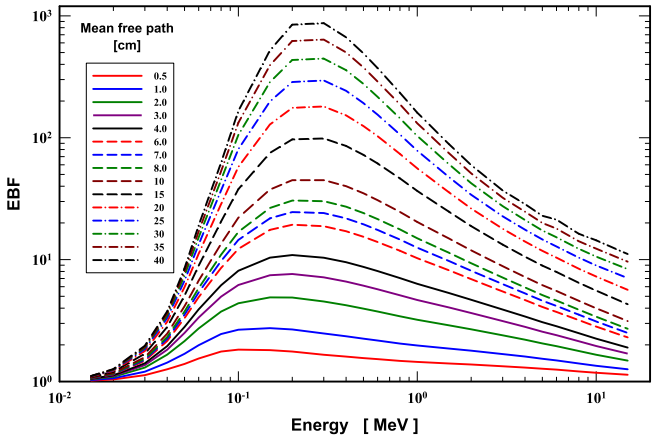

Fig. 3. EBF of cantera.

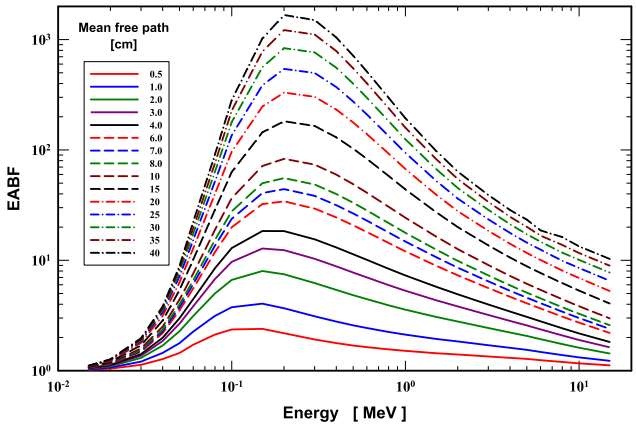

Fig. 4. EABF of cantera.

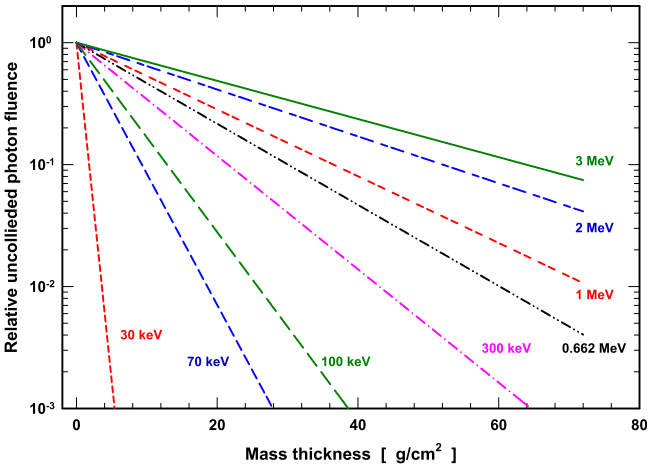

Fig. 5. Uncollided photon transmission in cantera.

Table 2
Linear attenuation coefficients of cantera, calculated with XCOM and MCNP5 codes.

Photon energy [MeV[	μ_{XCOM} [cm^{-1}]	μ_{MCNP5} [cm^{-1}]
0.030	2.2895	2.2920
0.070	0.4457	0.4455
0.100	0.3218	0.3219
0.300	0.1928	0.1926
0.662	0.1380	0.1379
1	0.1137	0.1135
2	0.0798	0.0797
3	0.0650	0.0649

In Fig. 6 the relative total photon (collided) transmission in cantera is shown. Total photon fluence includes the uncollided and the scattered photons. The differences between the photon transmission in Figs. 5 and 6 are due photon buildup in the detector. This build up is produced by photons that are scattered in the cantera reaching the detector.

In Fig. 7 the Ka transmission due to total photon fluence, in function of cantera mass thickness (x/ρ) for mono-energetic photons are presented. This feature is shown in terms of x/ρ because the density of cantera tuffs varies from 1.80 to 2.37 g cm^{-3} (López-Doncel et al., 2016).

The Ambient dose equivalent transmission of mono-energetic photons in cantera is shown in Fig. 8.

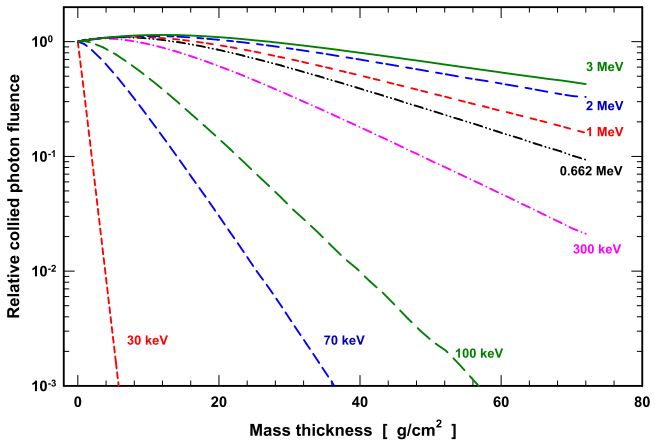

Fig. 6. Collided photon transmission in cantera.

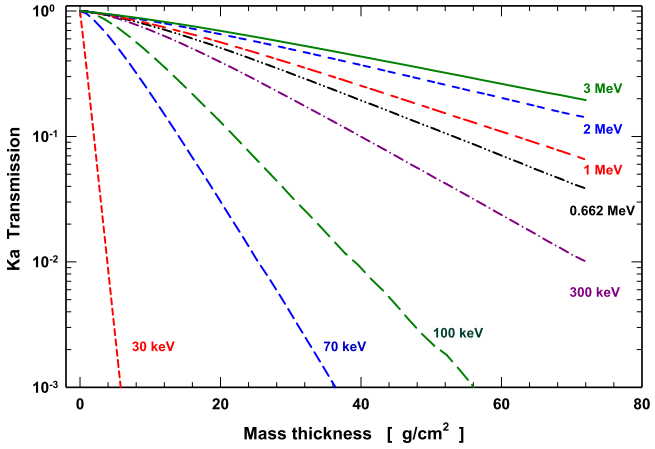

Fig. 7. Kerma in air transmission in cantera.

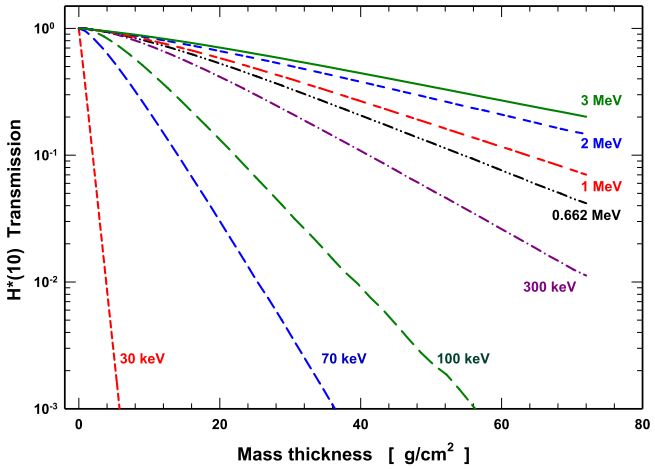

Fig. 8. Ambient dose equivalent transmission in cantera.

Despite the fluence-to-H*(10) conversion coefficients are larger than the fluence-to-Ka conversion coefficients for photons from 0.03 to 3 MeV (ICRP, 1996), for the same thickness of cantera the H*(10) transmission is slightly larger than Ka transmission. The probable explanation is because H*(10) and the Ka values were calculated using collided photons (uncollided and scattered) that

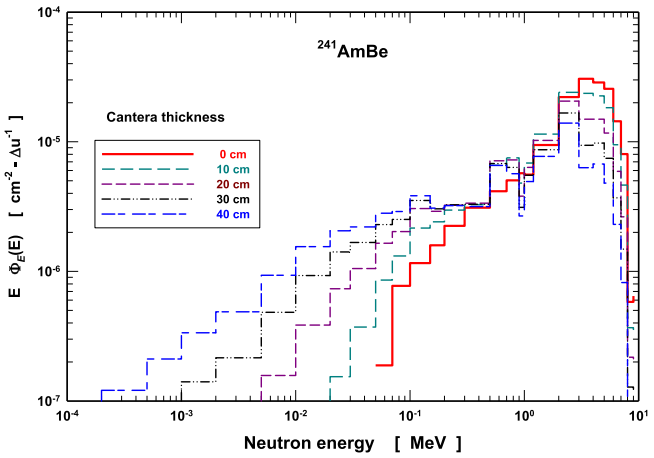

Fig. 9. Neutron spectra, per history, in function of cantera thickness.

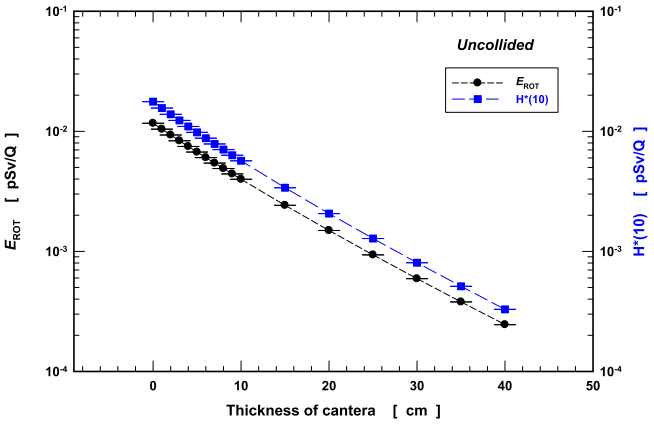

Fig. 10. E_{rot} and H*(10) reduction of ^{241}AmBe uncollided neutrons of cantera.

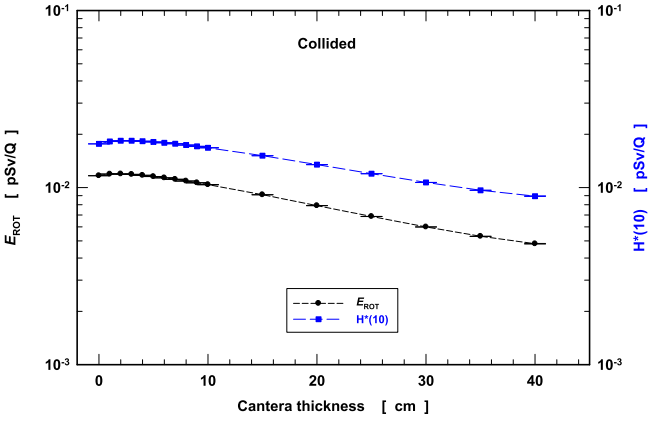

Fig. 11. E_{rot} and H*(10), per history, reduction of ^{241}AmBe collided neutrons of cantera.

reach the detector, therefore some scattered photons have energies where fluence-to-Ka conversion coefficients are larger than fluence-to-H*(10) conversion coefficients.

In Fig. 9 the neutron spectra, per history, of ^{241}AmBe in function of cantera thickness are shown. The spectra are the collided neutrons. Above 1.8 MeV neutrons are reduced as the cantera thickness is increased; however in the interactions neutrons lose energy reaching the point of interest with lower energies.

In Fig. 10 the E_{rot} and the $H^*(10)$, per history (Q), of uncollided neutrons from the ^{241}AmBe source, in function of cantera thickness, are shown.

Approximately 40 cm of cantera reduces two orders of magnitude both dosimetric quantities. This shielding feature is reduced when the collided neutrons are included, as is shown in Fig. 11.

Nevertheless neutrons above 1.8 MeV are reduced as the cantera thickness increases, in the interaction neutrons mainly lose energy, becoming epithermal reaching the point of interest and increasing the E_{rot} and $H^*(10)$. These dosimetric quantities are weakly reduced when the uncollided neutrons are used; therefore, cantera has limitations to be used to shield neutrons, because it do not contain light elements with good moderator properties.

3.2. Measurements

The linear attenuation coefficient of cantera for 0.662 MeV photons from ^{137}Cs source is 0.14 ± 0.01 cm^{-1}. This value was obtained through measurements carried out with the NaI(Tl) γ-ray spectrometer. The measured μ is in agreement with the μ-values for 0.662 MeV photons calculated with XCOM and MCNP5 codes, shown in Table 2. The μ/ρ for 0.662 MeV is 0.076 cm^2 g^{-1} being similar to the value shown in building materials (Mann et al., 2013) and is close to μ/ρ of aluminium (0.0747 cm^2 g^{-1}) and smaller than μ/ρ of lead (0.1101 cm^2 g^{-1}).

4. Conclusions

The cantera is widely used in the construction industry however, it's shielding features against x and γ-rays were unknown. Through calculations with XCOM and MCNP5 codes the shielding features of cantera have been estimated for 0.03, 0.07, 0.100, 0.300, 0.662, 1, 2, and 3 MeV monoenergetic photons. Using a ^{137}Cs and a NaI(Tl) γ-ray spectrometer the linear attenuation coefficient for 0.662 MeV photons was also measured.

Due to total alkali and silica content in this quarry tuff is defined as rhyolite having a density of 1.8 g cm^{-3}.

Linear attenuation coefficient of cantera varies from approximately 2.290 to 0.065 cm^{-1} for 30 keV to 3 MeV photons respectively. For 30 keV photons the HVL is 0.3 cm and 10.7 cm for 3 MeV γ-rays.

Photons with energy less than 60 keV are effectively shielded because the main interaction with cantera is through photoelectric interaction. Thus, the use of cantera in rooms with X-ray units for mammography contributes to reduce the dose.

For photons with energy between 60 keV and 20 MeV the main interaction in cantera is Compton scattering. Here, the energy of the incoming photon is reduced, but scattered photons contribute with the photon and the dose build up that should be evaluated. Nevertheless in rooms with X-ray units working above 60 kV, like dental or for diagnosis, or those with low-energy γ-rays sources, the cantera in the walls will help to shield photons and to reduce the dose.

For the same thickness of cantera, Ka and $H^*(10)$ transmission due to photons is almost the same.

Due to the lack of elements with good moderator features cantera is not a good shielding for ^{241}AmBe neutrons.

A limitation of this work was the use of monoenergetic photons to represent x-rays, because X-ray tubes produce photons with a wide and continuous energy distribution together with few discrete peaks where just quite few photons have the largest energy. However, if the information here presented is used to calculate a shielding made with cantera will be conservative because the photon mean energy of actual X-rays is smaller than the energy of photons here used. Other limitation is the lack of experimental evidence of cantera shielding characteristics against ^{241}AmBe neutrons.

Acknowledgments

This work is part of project SECuBo partially supported by the Universidad Autonoma de Zacatecas (UAZ-2015-36949).

References

ANS, 1991. Gamma ray attenuation coefficient and buildup factors for engineering materials. ANSI/ANS-6.4.3. American Nuclear Society, La Grange Park, Illinois.
Berger, M.J., Hubbell, J.H., Seltzer, S.M., Chang, J., Coursey, J.S., Sukumar, R., Zucker, D.S., Olsen, K., 2015. XCOM: Photon Cross Sections Database, version 1.5, [Online]. <http://physics.nist.gov/pml/data/xcom /data/xcom/index.cfm>. Gaithersburg, MD, USA.
Celik, M.Y., Ergul, A., 2015. The influence of the water saturation on the strength of volcanic tuffs used as building stones. Environmental Earth Science 74, 3223–3239.
Degerlier, M., 2013. Assessment of natural radioactivity and radiation hazard in volcanic tuff stones used as building and decoration materials in the Cappadocia region, Turkey. Radioprotection 48, 215–229.
El-Khayatt, A.M., 2017. Calculation of photon shielding properties for some neutron shielding materials. Nucl. Sci. Tech. 28, 69.
El-Khayatt, A.M., Ali, A.M., Singh, V.P., Badiger, N.M., 2014. Determination of mass attenuation coefficient of low Z dosimetric materials. Radiat. Eff. Defects Solids 169, 1038–1044.
Gallego, E., Lorente, A., Vega-Carrillo, H.R., 2009. Testing of a high-density concrete as neutron shielding material. Nucl. Technol. 162, 399–404.
Hadad, K., Nemathollahi, M., Sadeghpour, H., Faghihi, R., 2016. Moderation and shielding optimization for a ^{252}Cf based prompt gamma neutron activation analyser system. Int. J. Hydrogen Energy 41, 7221–7226.
Harima, Y., Tanaka, S., Sakamoto, Y., Hirayama, H., 1991. Development of new gamma-ray buildup factor and application to shielding calculation. J. Nucl. Sci. Technol. 28, 74–84.
IAEA, 2001. Compendium of neutron spectra and detector responses for radiation protection purposes. Technical report series No. 403. International Atomic Energy Agency, Vienna.
ICRP, 1996. *Conversion coefficients for use in radiological* protection against external radiation. ICRP Publication74. Annals of the ICRP. 179.
Kaewjang, S., Maghanemi, U., Kothan, S., Kim, H.J., Limkitjaroenporn, P., Kaewkhao, J., 2014. New gadolinium based glasses for gamma-rays shielding materials. Nucl. Eng. Des. 280, 21–26.
Kaur, P., Singh, D., Singh, T., 2016. Heavy metal oxide glasses as gamma rays shielding material. Nucl. Eng. Des. 307, 364–376.
Kurudirek, M., Ozdemir, Y., 2011. Energy absorption and exposure buildup factors for some polymers and tissue substitute materials: photon energy, penetration depth and chemical composition dependence. J. Radiol. Prot. 31, 117–128.
Le Bas, M.J., Le Maitre, R.W., Woolley, A.R., 1992. The construction of the total alkali-silica chemical classification of volcanic rocks. Mineral. Petrol. 46, 1–22.
López-Doncel, R., Wedekind, W., Leiser, T., Molina-Maldondo, S., Velasco-Sánchez, A., Dohrmann, R., Kral, A., Wittenborn, A., Aguillón-Robles, A., Siegesmund, S., 2016. Salt bursting test on volcanic tuff rock from Mexico. Environ. Earth Sci. 75, 212.
Mann, K.S., 2017. γ-ray shielding behaviours of some nuclear engineering materials. Nucl. Eng. Technol. 49, 792–800.
Mann, K.S., Singla, J., Kumar, V., Sidhu, G.S., 2012. Verification of some building materials as gamma-ray shields. Radiat. Prot. Dosimetry. 151, 183–195.
Mann, K.S., Kaur, B., Sidhu, G.S., Kumar, A., 2013. Investigations of some building materials for γ-rays shielding effectiveness. Radiat. Phys. Chem. 87, 16–25.
Mann, K.S., Rani, A., Heer, M.S., 2015. Shielding behaviours of some polymer and plastic materials for gamma-rays. Radiat. Phys. Chem. 106, 247–254.
Narici, L., Casolino, M., Di Fino, L., Larosa, M., Picozza, P., Rizzo, A., Zaconte, V., 2017. Polyethylene as radiation shielding on-board the International Space Station in high latitude radiation environment. Sci. Rep. 7, 1644.
Oto, B., Yildiz, N., Akdemir, F., Kavaz, E., 2015. Investigation of gamma radiation shielding properties of various ores. Prog. Nucl. Energy 85, 391–403.
Oto, B., Gur, A., Kavaz, E., Cakir, T., Yaltay, N., 2016. Determination of gamma and fast neutron shielding parameters of magnetite concretes. Prog. Nucl. Energy 92, 71–80.
Pérez, N.A., Lima, E., Bosch, P., Méndez-Vivar, J., 2014. Consolidating materials for the volcanic tuff in western Mexico. J. Cultural Heritage 15, 352–358.
Piotrowski, T., Tefelski, D.B., Sokolowska, J.J., Jaworska, B., 2015a. NGS-Concrete – New generation shielding concrete against ionizing radiation – the potencial evaluation and preliminary investigation. Acta Physica Polonica A 128, B-9–B-13.
Piotrowski, T., Tefelski, D.B., Skubalski, J., Zak, A., 2015b. Experiments on neutron transport through concrete member and the potential for the use in material investigation. Acta Physica Polonica A 128, B-14–B-18.
Sayyed, M.I., 2016. Investigation of gamma ray and fast neutron shielding properties of tellurite glasses with different oxide compositions. Can. J. Phys. 94, 1133–1137.

Singh, V.P., Badiger, N.M., El-Khayatt, A.M., 2014. Study on γ-ray exposure buildup factors and fast neutron-shielding properties of some building materials. Radiat. Effects Defects Solids 169, 547–559.
Turhan, S., Atici, E., Varinlioglu, A., 2015. Radiometric analysis of volcanic tuff stones used as ornamental and structural building materials in Turkey and evaluation of radiological risk. Radioprotection 50, 273–280.
Vega-Carrillo, H.R., 1989. Least squares for different experimental cases. Revista Mexicana de Física 35, 597–602.
Wally, E.-S.A., Fusco, M.A., Bourham, M.A., 2016. Gamma-ray mass attenuation coefficient and half value layer factor of some oxide glass shielding materials. Ann. Nucl. Energy 96, 26–30.
Waly, E.-S.A., Bourham, M.A., 2015. Comparative study of different concrete composition as gamma-ray shielding materials. Ann. Nucl. Energy 85, 306–310.
Wedekind, W., López-Doncel, R., Dohrmann, R., Kocher, M., Siegesmund, S., 2013. Weathering of volcanic tuff rocks caused by moisture expansion. Environ. Earth Sci. 69, 1203–1224.
X-5 Monte Carlo Team. 2003. MCNP – A General N-Particle Transport Code. Report LA-UR-03-1987 Los Alamos National Laboratory.
Zhang, F., Wu, H., Wang, X., Wu, G., Jia, W., Ti, Y., 2017. Compact shielding design of a portable ^{241}Am-Be source. Appl. Radiat. Isot. 128, 49–54.